Available online at www.sciencedirect.com

ScienceDirect

www.elsevier.com/locate/jes

JES JOURNAL OF ENVIRONMENTAL SCIENCES

www.jesc.ac.cn

Simultaneous degradation of sulfadiazine and dissolved organic matter based on low-impact development facilities

Donghai Yuan[1], *Siyu Xiong*[1], *Chenling Yan*[2], *Linxiao Zhai*[3], *Yanqi Cui*[1], *Yingying Kou*[1,*]

[1] *Key Laboratory of Urban Stormwater System and Water Environment, Ministry of Education, Beijing University of Civil Engineering and Architecture, Beijing 100044, China*

[2] *Beijing Key Laboratory of Municipal Solid Waste Detection Analysis and Evaluation, Beijing Municipal Institute of City Management, Beijing 100028, China*

[3] *ZC Daring (Beijing) Smart City Science and Technology Development Co. Ltd., Beijing 101100, China*

ARTICLE INFO

Article history:
Received 1 August 2022
Revised 8 October 2022
Accepted 9 October 2022
Available online 19 October 2022

Keywords:
Sulfadiazine (SD)
Low-impact development (LID)
Agricultural non-point sources
Dissolved organic matter (DOM)
Parallel factor analysis (PARAFAC)

ABSTRACT

Sulfadiazine (SD) is a common antibiotic administered to treat bacterial infections in livestock, and its fate and migration are greatly affected by dissolved organic matter (DOM). The soil infiltration system [a typical low-impact development (LID) facility] can significantly alter DOM properties during runoff pollution, thus affecting the complexation of SD with DOM. Here, the binding characteristics of different DOM components and SD in the soil infiltration system were explored using spectroscopic techniques (excitation–emission matrices, parallel factor analysis, and synchronous fluorescence spectroscopy). Combined with the weakening of DOM fluorescence intensity and 78.63% reduction in mean SD concentration following treatment, synchronous degradation may have occurred. The binding sequence of SD and DOM fluorophores was further explored using two-dimensional correlation spectroscopy. Effluent DOM showed greater sensitivity to SD and more binding sites than influent DOM. Moreover, hydrophobic protein-like substances exhibited higher log K_M values than other fluorescent components, indicating that protein-like components play significant roles in SD complexation. The soil percolation system improved the complexation stability and binding sequence of fulvic-like substances. Thus, SD–DOM can be intercepted and degraded using LID facilities to reduce the risk of SD in aquatic environments.

* Corresponding author.
E-mail: kouyy@bucea.edu.cn (Y. Kou).

https://doi.org/10.1016/j.jes.2022.10.010
1001-0742/

Introduction

Pharmaceuticals and personal care products (PPCPs) are widespread pollutants in the environment and have attracted increasing research attention worldwide because of their long-term negative impacts on the ecological environment (Luo et al., 2014). Sulfadiazine (SD) is one of the most commonly used antibiotics to treat bacterial infections in livestock. Owing to its high stability and hydrophilicity, the frequency of detection of SD in China's domestic hydrosphere exceeds 80% (Kokoszka et al., 2021). Typically, direct absorption and exertion of SD by animals is difficult; as such, approximately 50% of SD is excreted after use by humans and livestock (Sukul and Spiteller, 2006). Through migration and diffusion with stormwater runoff and other means, SD is detected at large quantities in soil, surface water, and groundwater (Chen et al., 2015; Hamscher et al., 2005; Sukul and Spiteller, 2006). However, the risk assessment of SD in aquatic environments remains insufficient.

Recent studies on SD mainly focused on surface water (Göbel et al., 2007) and wastewater from sewage treatment plants (Focazio et al., 2008). However, in agricultural non-point source pollution, the biological toxicity and migration risk of organic pollutants from soil to the hydrosphere, such as large amounts of antibiotic-contaminated poultry manure, have received limited attention. Previously, soil amelioration techniques have been proposed to effectively improve soil water purification capacity and remove organic pollutants through soil amendments (Zhou et al., 2018). These methods can reduce the degree of pollution from the source and can be implemented at the large-scale for domestic sewage treatment in rural areas. However, few related studies have explored SD migration characteristics in agricultural non-point source pollution runoff and the associated environmental risks.

Soil infiltration technology is an essential measure for solving the problem of non-point source pollution. By intercepting and adsorbing runoff pollutants, the system can reduce organic pollutants, including PPCPs, by affecting their mobility and reducing their potential risks. As a low-impact development (LID) facility, the soil infiltration system produces an excellent purifying effect on the quality of runoff water (Yuan et al., 2019). Most previous studies have focused on conventional pollutants in urban runoff while neglecting the degradation of agricultural non-point source pollutants, particularly organic ones. Soil infiltration systems have been proven to control runoff pollution (Tedoldi et al., 2016). However, only a few studies have explored the control effects of this facility on agricultural runoff pollution and its impact on the migration of novel pollutants, particularly SD (Yuan et al., 2019).

Photodegradation is an emerging technology for the removal of antibiotic residues in aquatic environments (Wu et al., 2018), and diverse strategies have been proposed to improve photocatalytic efficiency, such as facet heterojunctions (Bao et al., 2016) and carbon quantum dots (Liang et al., 2018). In addition to direct photodegradation caused by the sunlight, dissolved organic matter (DOM) in the environment can mediate indirect photodegradation of PPCPs (Li et al., 2017). Upon absorbing light, DOM can induce the formation of reactive intermediates, such as hydroxyl radicals (•OH) and excited triplet states of DOM (^{3}DOM*), which can promote indirect photodegradation of PPCPs (Bai et al., 2021). DOM is a specific photosensitizer in the natural environment, which not only promotes antibiotic photodegradation but also prevents secondary environmental pollution (Awual et al., 2014). Therefore, DOM characteristics during SD degradation warrant further attention.

Spectroscopic techniques, including synchronous fluorescence spectroscopy (SFS) and three-dimensional fluorescence excitation–emission matrices (EEMs), are typically used to track the component types and sources of DOM (Yuan et al., 2018). Therefore, these methods are effective for analyzing possible changes in complexation mechanisms between SD and DOM before and after flowing through the soil infiltration system. Exploration of these complexation mechanisms can help us better understand the impact of DOM on the migration and transportation of SD in non-point source pollution and the degradation effect of the soil infiltration system.

Aiming at solving the problem of paucity of research on the migration of PPCPs in agricultural non-point source pollution, in the present study, we explored the purification process of SD in runoff pollution through a typical LID facility and examined the removal effects and mechanisms of SD in agricultural non-point source pollution based on the soil infiltration system. The purpose of the present study was to (a) use spectroscopic techniques for verifying whether DOM and SD are simultaneously degraded before and after the soil infiltration treatment; (b) explore the effects of composition changes in the complexation process of DOM and SD before and after the soil infiltration treatment on the migration of SD in agricultural non-point sources pollution; and (c) provide a scientific basis for the treatment of PPCPs in agricultural non-point source pollution.

1. Materials and methods

1.1. *Experiments and samples*

The experimental device was located at No. 15 Yongyuan Road in Daxing, Beijing. The device comprised two parts: a percolation tank and a water distribution system (**Fig. 1**).

The percolation tank simulated the location of non-point source run-off migration. It is a rectangular PVC tank measuring 300 mm × 300 mm × 600 mm and possesses an opening at the bottom or collecting rainwater runoff. To prevent soil erosion, a layer of permeable geotextile is placed above the plate with the opening, and an overflow port is provided at the top. The runoff water distribution system is a 10 L glass water tank with a small submersible pump and rotameter.

The target of improvement was soil from the Baiyangdian Basin in the Hebei Province of northern China. According to previous reports, SD has been detected at considerable concentrations in the soil of this basin; therefore, allocating pollution sources and minimizing the potential risks are urgent issues (Yang, 2021). Soil amendment applied in the present ex-

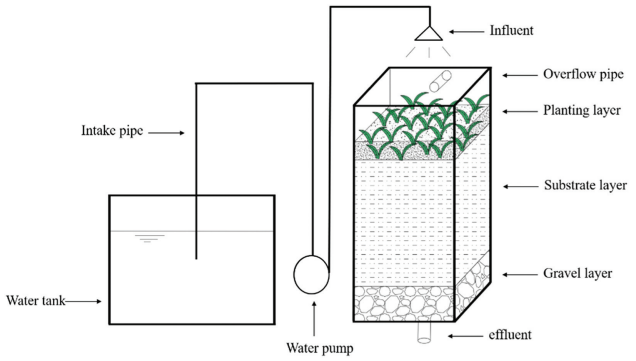

Fig. 1 – Soil infiltration device for simulating agricultural non-point sources run-off process.

Table 1 – Basic physical parameters of soil used in this study

Physical parameters	Soil[a]
pH	7.27 ± 0.23
Organic matter (g/kg)	11.07 ± 2.3
Conductivity (mS/cm)	9.07 ± 1.14
Particle size (D50) (μm^{-1})	21.9 ± 3.22
Water content (%)	15.55 ± 2.29
Zeta (mV)	6.4 ± 3.3

[a] All these values are the means of three replicates

periment included a 2–4 mm layer of zeolite and a 2–4 mm layer of ceramsite at a 1:1 ratio. The tank was filled with 450 mm of soil, and the amendment was added to the soil at a weight ratio of 10%, with thorough mixing and filling, covering 5 mm of the vegetation soil layer. To better explain the effect of the soil infiltration system on simultaneous degradation of SD and DOM, basic physical parameters of the soil samples were determined (**Table 1**).

Specifically, influent (I1) simulated the water distribution of agricultural pollution, and SD was added to observe the changes in DOM in the device. SD with >99% purity was provided by the Sinopharm Group. All water samples were evenly mixed and stored in a pre-cleaned polyethylene bucket at 4°C. Typically, the SD concentration of natural waters is 0.5 μg/L to 0.05 mg/L (Hamscher et al., 2005). To ensure that the quenching effect was easy to observe, SD concentration in the experiment was set to 9.63 μg/L, which is higher than that in natural water bodies. The experiment was run in quintuplicate, and the same SD concentration was added to the distribution tank to fully react with the simulated water distribution. The influent was fed into the treatment system at a constant flow rate (12.27 mL/min for 2 hr) to simulate the rainfall process that occurs once in 2 years and to ensure the same total runoff. After flowing through the processing unit, three sets of water samples were collected from the water outlet until the effluent flow was stable, and the average value was obtained. SD concentration was measured using high-performance liquid chromatography (Agilent 1260) with Waters Acuity UPLC BEH C20 (20 μL at 1 mL/min). Moro rover, Cu, Zn, and Cd concentrations were determined using flame atomic absorption spectrophotometry (FAAS; Z-2000). All water samples were passed through a 0.45 μm membrane to obtain DOM samples.

1.2. *Fluorescence quenching titration*

To minimize the inter-filtering effect, all samples were diluted with Milli-Q water to reduce total organic carbon (TOC) concentration to 10 mg C/L. Before the test, H^+ exchange resin was used to remove free heavy metal ions to eliminate the interference of heavy metal complexation with DOM. Next, 10 mL of the treated water sample was placed in a 20 mL sealed brown vial. Before titration, pH of the SD–DOM samples were adjusted in the range of 7.0 ± 0.02 using low concentrations of NaOH and HNO_3 (0.1 mol/L, $V < 100$ μL). SD was added to the pretreated SD–DOM samples for titration. The final concentration gradient of SD in the SD–DOM samples was 0, 20, 40, 60, 80, 100, 120, 150, and 200 μmol/L. To eliminate the effect of SD concentration, the volume of the SD solution added was maintained below 5% of the DOM sample volume. SD concentration in the surface water environment is relatively low (typically in ppb). To better understand the characteristics of DOM binding SD, SD concentrations used in the present experiment were relatively high. After titration, the SD–DOM samples were placed in a constant-temperature shaking box at 25°C and oscillated for 24 hr to ensure the balance of reaction complexation.

1.3. *Spectral measurements*

The EEMs of the DOM samples were determined in a 10 mm quartz cuvette at 20–25°C using a fluorescence spectrophotometer (F-7000, Hitachi, Japan) equipped with a 150 W xenon arc lamp as a light source. Excitation (Ex) and emission (Em) wavelength ranges were 200–450 and 280–550 nm, respectively, with a slit width of 5 nm for excitation and emission monochromators, and the scanning speed was 240 nm/min. A blank solution (Milli-Q) was used to subtract the spectrum of each sample to eliminate the interference of Raman and Rayleigh scattering (Guo et al., 2014b; Wei et al., 2016). In the present study, 60 EEMs were collected from the influent and effluent water with the soil infiltration treatment (**Fig. 2**) and the excitation and emission loads determined based on a four-component PARAFAC model were explained. SFS was used to obtain excitation and emission wavelengths with a constant offset ($\Delta\lambda = 55$ nm) and a slit width of 5 nm. The scanning speed and range were 240 nm/min and 250–500 nm, respectively.

1.4. *PARAFAC*

PARAFAC was performed using the DOMFluor toolbox operation of MATLAB 8.0. This analysis is mainly used for solving numerous stacked EEMs in which separating overlapping peaks as single fluorescent components is difficult. PARAFAC can be used for qualitative and quantitative analysis of DOM samples (Zhou et al., 2018). Specifically, it can be used to model a set of tens to dozens of EEM datasets and identify three to seven independent components based on diagnostic

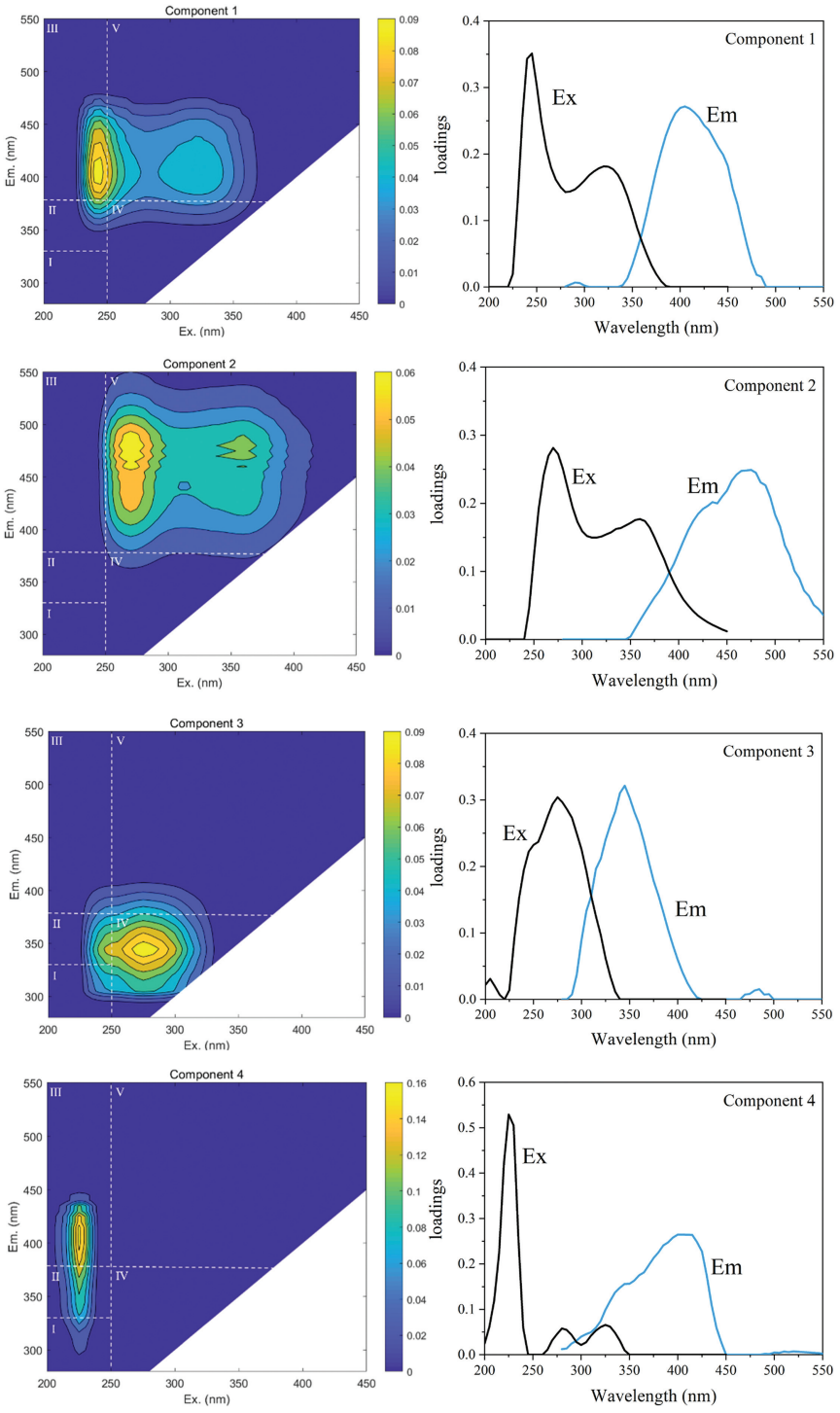

Fig. 2 – Fluorescent components, excitation (black lines) and emission loadings (blue lines) identified by the PARAFAC model. Initial pH=7.12; contact time=24 hr; initial SD concentration=9.63 μg/L.

tools, such as segmentation, semi-verification, and core consistency testing (Ohno and Bro, 2006). All data are analyzed based on fluorescence information using the maximum fluorescence intensity (F_{max}) value. The evaluation of EEM can finally be accurately decomposed into several independent components (Guo, 2014b). In the present study, the EEM data used for PARAFAC analysis included 60 samples per batch (30 for influent and 30 for effluent samples).

1.5. *Principal component analysis (PCA)*

PCA is a multivariate statistical method widely used to extract common features from datasets. Combined with the PARAFAC

model, PCA can explain majority of the changes in DOM components and identify DOM constituents. PCA was performed in SPSS 18.00 (SPSS International, Chicago, USA), and F_{max} data were subjected to PARAFAC. Because the analysis results may be affected by the non-independence of the spectral data, the Kaiser–Meyer–Olkin (KO) test was applied to determine inter-correlations. Regression and correlation analyses were performed using Origin 8.0 (OriginLab, Los Angeles, USA) and SPSS 18.00 (SPSS International). The significance level was divided into weak correlation (NS) ($p > 0.05$), general significance ($0.05 < p < 0.01$), or high significance ($p < 0.01$). In the present study, PCA was applied for in-depth mining of information on individual components of DOM and identification of the dominant component.

1.6. Two-dimensional correlation spectroscopy (2D-COS)

2D-COS can improve the spectral resolution by capturing and extracting subtle changes hidden in the featureless UV–Vis absorption spectrum. 2D-COS is widely used to study the interactions between DOM and heavy metals or organic pollutants, typically in conjunction with SFS and Fourier-transform infrared spectroscopy to analyze the binding sequence and sites (Lee et al., 2021). Here, we used SFS combined with 2D-COS to better understand the heterogeneity of binding sites and identify overlapping peaks.

1.7. Nonlinear complex model analysis

The Ryan–Weber (R–W) model is a commonly used nonlinear fitting model to calculate the complex constant of DOM samples and SD and then determine the strength of SD and DOM complexation (Ryan and Weber, 1982). This model is primarily based on the following assumptions: (1) SD and DOM have the same independent binding sites or ligand binding and (2) the stoichiometric ratio of SD to the ligand complex is 1:1. The R–W model can be given using Eq. (1), as follows:

$$I = I_0 + (I_{ML} - I_0)\left(\frac{1}{2K_M C_L}\right) \times\left(1 + K_M C_L + K_M C_M - \sqrt{(1 + K_M C_L + K_M C_M)^2 - 4K_M^2 C_L C_M}\right) \quad (1)$$

where I_0 is the DOM fluorescence intensity of the water sample without SD, C_M is the SD concentration, I is the fluorescence intensity at the SD concentration of C_M, C_L is the complexing capacity concentration of SD, and K_M is the SD complexing stability constant.

Simultaneously, I_{ML} indicates the concentration threshold of SD when the fluorescence intensity stabilizes; f is expressed as the quenching rate, that is, the ratio of the binding group to the total group, calculated using Eq. (2):

$$f = \frac{(I_0 - I_{ML})}{I_0} \quad (2)$$

2. Results and discussion

2.1. Changes in water quality parameters

Changes in the quality parameters of water influent and effluent in the process of simulating agricultural non-point source pollution runoff are summarized in **Table 2**. After three sets of parallel injections and addition of heavy metal ions (Cu^{2+}, Cd^{2+}, and Zn^{2+}) and SD to the water, the concentrations were 22.71, 24.09, 23.18, and 9.64 μg/L respectively, which were added to the distribution tank to completely react with the simulated water distribution. Major factors affecting the purification of pollutants in the soil infiltration system via the filler were related to the precipitation of certain pollutants. Mineral materials can purify water through adsorption and filtration or through ion changes and chemical activity (Song et al., 2012). **Table 2** presents changes in water quality parameters based on the measurement of heavy metal and SD concentration in the influent/effluent water and the conventional water quality indicators [e.g., TOC, total nitrogen (TN), and total phosphorus (TP)]. After passing through the system, the concentrations of TOC, TN, and TP decreased by 94.07%, 57.71%, and 93.61% respectively, indicating that the soil infiltration system could effectively improve the water quality in the runoff process. Moreover, the degradation rate of Cu^{2+}, Cd^{2+}, and Zn^{2+} reached 87.97%, 96.06%, and 91.67%, respectively. This degradation performance of the infiltration system for the above-mentioned pollutants is consistent with previous conclusions regarding the use of soil amendments to purify runoff rainwater pollutants. In a previous study, we illustrated that the system filler shows a more microporous structure and higher chemical stability, which can increase soil permeability and reduce soil cohesion (Yuan et al., 2019). This structural feature can be attributed to the effective removal of pollutants in the water by the infiltration system in our experiment. Compared with previous reports, the system with modifiers exhibited a greater degradation efficiency and stability, indicating that the improved soil infiltration system produced a better degradation effect on runoff pollutants. In particular, the average SD degradation rate from multiple measurements was 78.63%. This degradation effect may be related to other factors, such as pH. pH significantly affects the forms of DOM and PPCPs (Bai et al., 2018). The indirect photolysis rate of SD first increased and then decreased at different pH values ranging from 5 to 11, peaking at a pH of 7 (Liu et al., 2018). The present study only explored SD degradation under a pH of 7. Therefore, the effect of pH on DOM components and SD degradation requires further study.

The simultaneous decline in TOC and SD concentrations indicates possible interference in the complexation between SD and DOM during the runoff process, which can be confirmed by analyzing the changes in DOM composition (Bai et al., 2021).

2.2. Changes in PARAFAC components following soil infiltration treatment

The PARAFAC model can provide qualitative information on DOM and determine its fluorescent components (Yao

Table 2 – Concentrations of TOC, TN, TP, HMs and SD by LID

Sample	TOC mg/L	TN	TP	Cu^{2+} μg/L	Zn^{2+}	Cd^{2+}	SD
Influent	125.16(±3.78)	9.72(±3.11)	1.72(±0.21)	22.71(±0.74)	23.18(±1.73)	24.09(±2.11)	9.64(±2.66)
Effluent	7.45(±5.22)	4.11(±2.12)	0.11(±0.06)	2.73(±0.71)	1.93(±0.83)	0.95(±0.64)	2.06(±1.06)

[a]All these values are the means of three replicates.TN: total nitrogen; TP: total phosphorus; HMs: heavy metals; SD: SD; LID: low impact development.

et al., 2016). The excitation spectrum with peaks and the emission spectrum with a single peak are shown in **Fig. 2**. The four identifiable components could be classified into two humic-like components (C1 and C2), a protein-like component (C3), and a fulvic-like component (C4).

C1 showed two fluorescence peaks located at Ex/Em = 245/403 and 320/403 nm, similar to the typical terrestrial humic-like fluorescence (HLF) peak A (Baghoth et al., 2011; Yuan et al., 2017). The fluorescence peaks of C2 and C1 were similar, although C2 showed a wider range and an obvious red shift than C1. C2 showed a major fluorescence peak at Ex/Em = 275/480 nm and a sub-fluorescence peak at Ex/Em = 360/480 nm. These signals represent terrestrial humic-like substances (Coble et al., 1996; Petrone et al., 2011), such as high-molecular-weight and aromatic terrestrial organic matter (Yuan et al., 2018). C3 exhibited a fluorescence peak at Ex/Em = 280/340 nm, indicating a higher excitation and emission maxima than that of C1. This type of fluorescence signal may originate from land-based material contained in feces, reflecting the biodegradability of DOM. This fluorescence peak was attributed to a protein substance, possibly a tryptophan-like substance (Wang et al., 2020). The tryptophan-like peak T is commonly detected in samples from marine and terrestrial water environments (Yao et al., 2011). C4 showed the maxima of Ex/Em = ≤225/410 nm, similar to the peak A fluorescence peak signal of fulvic-like substances (Wang et al., 2020).

To further determine the major components of DOM and prevent errors in component identification due to Rayleigh scattering, PCA was performed on the relative abundance of PARAFAC components. The KMO and Bartlett sphericity tests (P) were applied to assess the feasibility and validity of PCs. PCA showed weak partial correlations among variables (KMO = 0.731) with a high performance (P = 0.01). In general, if the KMO value is exceeds 0.5 and the P value is below 0.05, PCA is considered feasible (Guo et al., 2014a). All components were analyzed to obtain two PCs, accounting for 90.327% of the total variance. F1 and F2 accounted for respectively 72.672% and 17.655% of the total variance in fluorescence components. All PCA factors were linear combinations of four DOM components, and the measurement factors presented no dimensions.

$$\text{Factor1} = 0.329C1 + 0.330C2 + 0.238C3 + 0.264C4 \quad (3)$$

$$\text{Factor2} = -0.066C1 - 0.049C2 + 0.949C3 - 0.213C4 \quad (4)$$

According to Eqs. (3) and (4), the four components simultaneously showed positive loads in F1. The humic-like

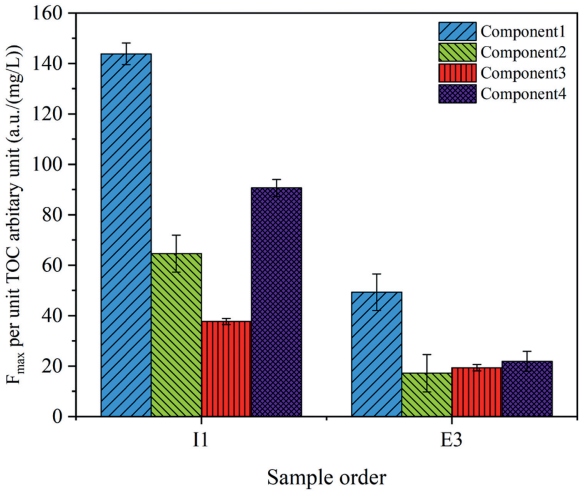

Fig. 3 – Fluorescence intensity distribution diagram of DOM components Influent and effluent water.

fluorescent components C1 and C2 showed significantly higher factor loads, indicating that in F1, the humic-like substances occupied the leading position. The only difference was that the tryptophan-like component C3 in F2 showed a positive load, indicating that F2 is mainly dominated by protein-like substances. Overall, PARAFAC and PCA revealed the characteristics of the DOM components in the present study, namely the source strength of humic-like components *versus* the contribution of protein-like components to the total fluorescence (Guo et al., 2015). Perhaps, these components originated from domestic sewage and aquaculture wastewater from agricultural non-point sources (Yao et al., 2011).

The EEM spectra of DOM extracted from samples after titration with different concentration of SD in influent water (Appendix A **Fig. S1**). The results showed that with the increase of SD concentration, the fluorescent components in DOM had a significant quenching effect, which indicated that the combination of DOM and SD changed the structure of DOM. Besides, the EEM spectrum of DOM in effluent water shows a different quenching phenomenon (Appendix A **Fig. S2)**. Although affected by the adsorption of soil infiltration system, the fluorescence intensity of DOM components in effluent decreased, but with the change of SD concentration, the quenching laws of different components were different.

The main F_{max} values for each component after the treatment are presented in **Fig. 3**. DOM components were separated based on the PARAFAC model. Analysis of all water samples

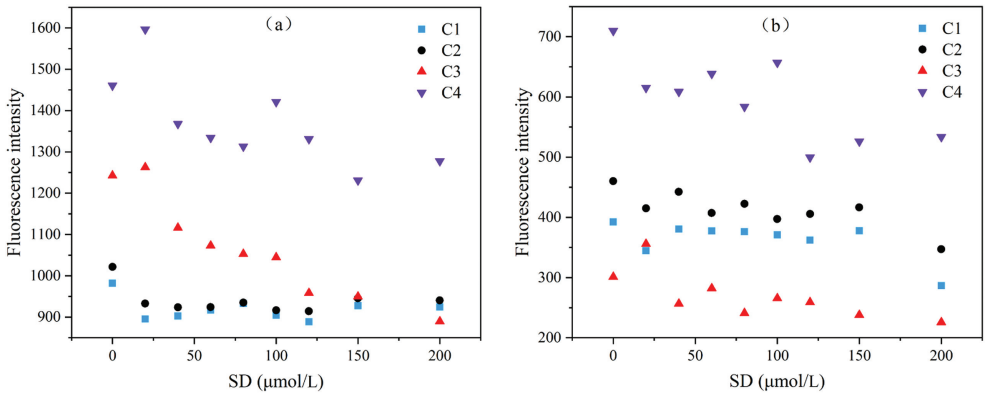

Fig. 4 – Influent (a) and effluent (b) fluorescence quenching curves of each PARAFAC derivative component of SD titration (0-200 μmol/L). Initial pH=7.0 ± 0.02.

indicated that the F_{max} values of the two terrestrial humus components were significantly higher than those of the protein components. The fluorescence component scores of C1, C2, C3, and C4 in the untreated water sample (I1) were 42.70%, 19.18%, 11.19%, and 26.93%, respectively. Thus, in agricultural non-point source pollution, high-molecular-weight and aromatic terrestrial organic matter content is higher. A higher concentration of humus compounds implies that the water quality is more prone to humification, and this water more likely to cause eutrophication and black odor upon entering the surface water environment through runoff. Compared with the untreated influent (I1), samples subjected to the soil infiltration treatment (E3) showed different degrees of reduction in the fluorescence intensity of each component of DOM in the water body. As shown in **Fig. 3**, most of the removed components were fulvic-like (C4), and their degradation rate was as high as 76.5%. In addition, the humic-like substances C1 and C2 were significantly reduced following the infiltration treatment, and their degradation rates reached 65.7% and 72.5%, respectively. Although the degradation rate of tryptophan components (C3) was slightly lower than that of C1 and C2, it still reached ~54.3%.

The above results may be explained as follows. The filler structure of the treatment provides space for the growth and metabolism of microorganisms and increases the absorption and utilization of organic pollutants in agricultural non-point source pollution (Yuan et al., 2018). Thus, the degradation efficiency of high-molecular-weight humus and fulvic-like components was high. Furthermore, the degradation of DOM components affects the migration and transformation processes of SD. Overall, based on the identified DOM components and changes in their concentrations between the influent and effluent, we can preliminarily explain that the migration and transformation of SD are accompanied by changes in DOM components. Although the SD degradation mechanism may primarily depend on adsorption and soil type (Yuan et al., 2019), SD–DOM changes in pollutants in water samples before and after passing through the system must be studied.

The quenching curves of the four DOM components in influent and effluent of the treatment are shown in **Fig. 4**. As shown in **Fig. 4a**, large differences in quenching performance were noted between SD and the different DOM components. Specifically, C3 and C4 showed obvious quenching effects with increasing SD concentration, consistent with previous reports (Wang et al., 2020). Meanwhile, the quenching effects of C1 and C2 changed with increasing SD concentration, indicating poor complexation between humic-like components and SD. Previous studies have shown that PPCP pollution is typically less intense when binding to hydrophilic than to hydrophobic components of DOM (Hernandez-Ruiz et al., 2012). As a hydrophobic component, protein-like C3 showed a greater degree of quenching than the hydrophilic C1 and C2, which is consistent with the above conclusion. Furthermore, the combination of hydrophobic protein-like substances and SD plays a vital role in the migration and transformation of SD. Therefore, the change in C4 may have resulted from a cationic bridge between deprotonated carboxyl groups, irrespective of the DOM type.

The fluorescence intensity of each DOM component in effluent was reduced **(Fig. 4b)**, which may lead to changes in the mechanism of complexation between the SD and DOM. The degree of quenching of C1 and C2 did not differ significantly between the influent and effluent water, indicating that the complexation of terrestrial humic-like substances with DOM is not affected by soil infiltration. Although the fluorescence intensities of C3 and C4 decreased, they continued to show strong quenching. Therefore, the strong complexation between protein-like substances and SD was not affected by changes in protein-like substances. Meanwhile, the low correlation between the quenching and fluorescence intensities of fulvic-like particles was consistent with the trend noted for influent. Based on changes in the quenching titration of SD and DOM components, differences in the complexing ability of the different components with SD are presented in **Fig. 4**. Overall, the SD migration process in the soil infiltration system was affected by fulvic-like and protein-like components of DOM, and these components formed relatively stable complexes with SD. However, sequential changes in the complexation of DOM and SD and sensitivity changes to the infiltration system of this complexation must be explained with additional information. Based on the quenching curves and degradation rates of DOM components, SD can be removed by DOM. Overall, the binding site heterogeneities of SD–DOM may be affected by the soil infiltration treatment.

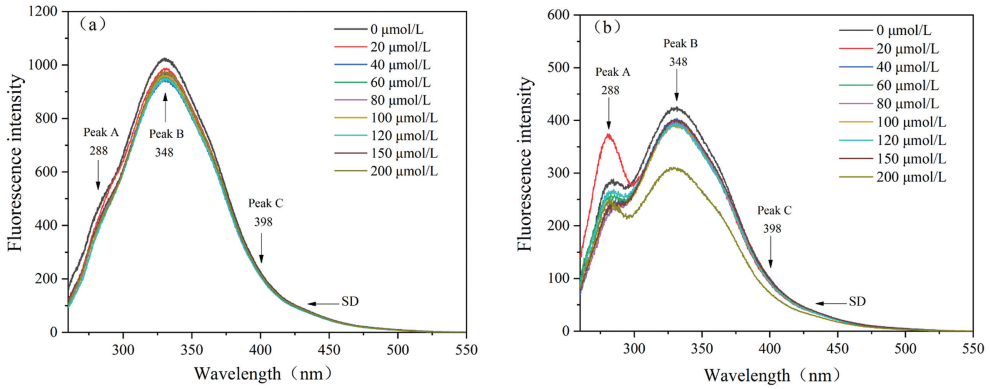

Fig. 5 – Synchronous fluorescence spectra of influent DOM (a) and effluent DOM (b) with increasing SD concentration (0-200 μmol/L). Initial pH=7.0 ± 0.02.

2.3. *Combining characteristics of SD-DOM*

As shown in **Fig. 5**, the synchronous fluorescence spectra of DOM in the influent and effluent water following the soil infiltration treatment showed a peak at 288 nm (Peak A), expressed as a protein-like fluorescence (PLF) peak, which was related to aromatic (tryptophan-like or tyrosine-like) amino acids or other nitrogen-containing groups. Peak B was detected at 348 nm and was related to a fulvic-like fluorescence (FLF) signal. Peak C at 398 nm was a typical HLF signal (Huang et al., 2020). In influent DOM (**Fig. 5a**), with increase in SD concentration, Peak B exhibited a relatively obvious quenching phenomenon, which is typically observed in the case of polar functional groups (Navon et al., 2011). Peak A showed a certain degree of attenuation of fluorescence intensity, which was related to the combination of hydrophobic components of protein-like fluorophores with SD. The quenching phenomenon of peak C was not obvious. This phenomenon is consistent with the quenching of components revealed by PARAFAC.

As shown in **Fig. 5b**, the fluorescence intensity of HLF, FLF, and PLF was greatly reduced, indicating that the interception or degradation of DOM by an enormous number of soil infiltration systems. Simultaneously, the fluorescence quenching effect of different substances of DOM was significantly different from that of water, indicating that during the process of SD and DOM complexation, the electronic structure of DOM changed and the fluorescent groups were affected by SD. Therefore, the effects of combination showed differences in quenching. Comparison of the SFS spectra of influent and effluent water revealed that the quenching effect at 288 nm was greater than that at 348 and 398 nm, indicating that the hydrophobic interaction between DOM and SD was a dominant factor in SD–DOM complexation, whereas the hydrophilic interaction mostly occurred between the ionization part of SD and the carboxyl groups of DOM (Guo et al., 2018).

To study the binding site and sequence of DOM fluorophore and SD, SFS was combined with 2D-COS, and visualized stereo images were used to better present the complexation characteristics of DOM and SD. Two spontaneous peaks were detected in the influent water **(Fig. 6a**) located at 275 nm and 325 nm, representing the sensitivity of spectrum intensity fluctuations to disturbances in external conditions. The stronger the spontaneous peak, the more sensitive the SD is to the external environment. In addition, two positive crossover peaks were detected at 295/275 and 320/275 nm. Fluorescence intensity at different wavelengths reflects the sensitivity of DOM to SD interactions (Noda and Ozaki, 2005). The order of peak intensity was 320/275 nm→295/275 nm, indicating that proteinaceous substances were more susceptible to SD concentration. The result shown in **Fig. 6c** is similar to that for influent, with two spontaneous peaks detected at 280 and 340 nm, but no cross-over peaks. Following the soil improvement treatment, peak intensity was reduced although the quenching effect of SD on DOM remained unchanged. Meanwhile, the fluorescence quenching effect of SD on protein components was stronger than that of water. Overall, the fluorescence spectra confirmed that soil infiltration could affect the complexation of SD and DOM in the treatment of agricultural non-point source pollution.

The 2D-COS map of asynchronous binding shows the sequence of changes in the binding sites of SD and DOM. As shown in **Fig. 6b**, the influent showed three orthogonal peaks (280/270, 288/270, and 295/285 nm) and four negative cross-over peaks (285/280, 326/298, 326/278, and 348/277 nm). According to Noda's law (Noda and Ozaki, 2005), the order of combination of DOM and SD is 288/270 nm→280/270 nm→295/285 nm→285/280 nm→326/278 nm→348/277 nm→326/298 nm, which indicates that protein-like fluorescent components complex with SD earlier than fulvic-like or humic-like substances. After the soil improvement treatment, the number of DOM binding sites was significantly reduction. **Fig. 6** presents asynchronous 2D-COS results for water, with three positive cross-over peaks at 348/280, 326/278, and 352/280 nm and a negative cross-over peak at 280/273 nm. The binding sequence of DOM to SD was 348/280 →325/280 →352/280 →280/273 nm, indicating that after the soil infiltration treatment, the sensitivity of fulvic-like structures to SD and their affinity for SD complexation increased. Therefore, DOM could reduce SD concentration to a certain extent. Simultaneously, the soil infiltration system increased the sensitivity of DOM to SD and altered the binding site and sequence of SD–DOM.

2.4. *SD-DOM combined parameters*

Table 3 shows the complex stability constant of DOM–SD obtained using the R–W model combined with synchronous fluorescence spectrum fitting. The complex stability constant

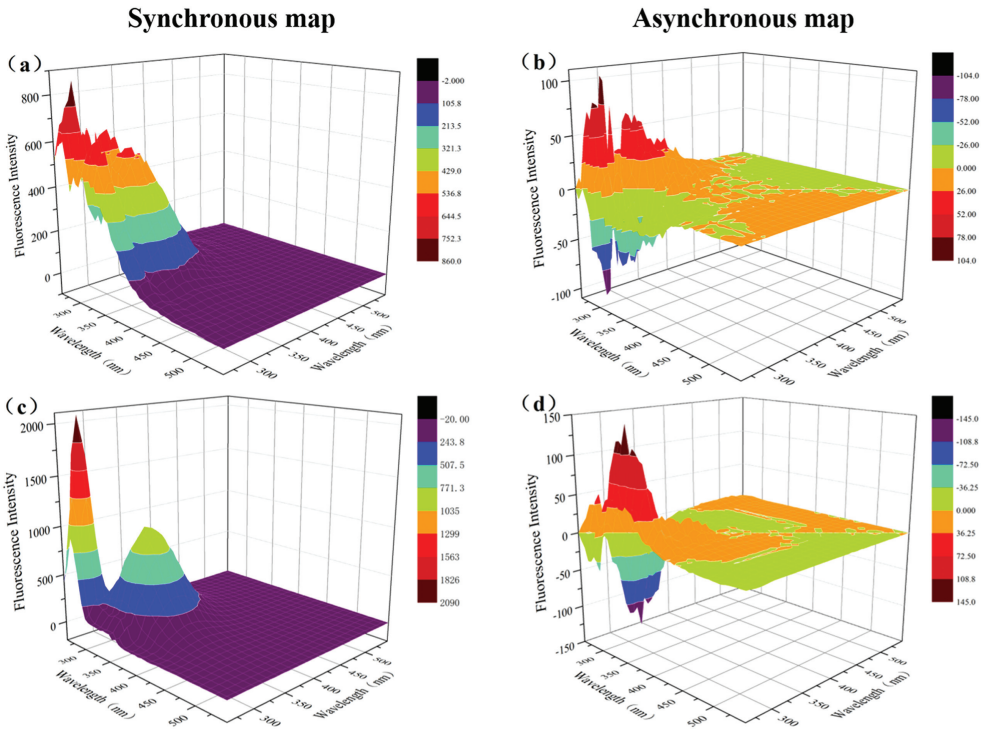

Fig. 6 – Obtain a visualized 2D-COS graph from the synchronous fluorescence spectra of SD-DOM in the influent (a, b) and effluent (c, d). Initial pH=7.12; contact time=24 hr; initial SD concentration=9.63 μg/L.

Table 3 – Ryan-Weber model fitting represents the SD-DOM complex stability constant

I4				E3			
Wavelength (nm)	logK_M	f	R^2	Wavelength (nm)	logK_M	f	R^2
288 [a]	3.17	0.92	0.979 [b]	288	3.59	0.67	0.892 [b]
326 [a]	3.22	0.88	0.986 [b]	326	3.81	0.57	0.998 [b]
348 [a]	3.19	0.53	0.943 [b]	348	3.51	0.43	0.931 [b]
398 [a]	3.21	0.35	0.851 [b]	398	3.34	0.28	0.886 [b]

[a] These peaks can be identified by the 2D-SFS-COS maps.
[b] Correlation is significant at p = 0.01 level (2-tailed).

Table 4 – Stability constants and quenching rates of DOM components complexed with SD

Components	I4			E3		
	logK_M	f	R^2	logK_M	f	R^2
C2 [a]	3.17	0.08	0.974 [b]	3.48	0.25	0.981 [b]
C3 [a]	3.62	0.28	0.986 [b]	3.77	0.24	0.993 [b]
C4 [a]	3.35	0.13	0.983 [b]	3.39	0.25	0.985 [b]

[a] These peaks can be identified by the 2D-SFS-COS maps.
[b] Correlation is significant at p = 0.01 level (2-tailed).

(logK_M) of SD–DOM was in the range of 3.17–3.81. The complexation stability of each component of 2D-COS after soil infiltration treatment, arranged in the order from large to small, was as follows: protein substances → fulvic-like substances → humic-like substances (288 → 348 → 398 nm; **Fig. 6**). Protein substances showed a higher logK_M value than humic-like substances, indicating that the complexes formed by protein substances and SD were more stable and followed a more consistent trend in the influent and effluent. The complexation constants of fulvic-like substances in the effluent increased significantly, consistent with the changing trends of the binding site sequence, indicating improved binding ability of fulvic-like substances to SD and altered complexing ability of these substance. Therefore, improvement of the soil filtration system is an important factor to reduce the risk of SD entering the aquatic environment.

Table 4 lists the $\log K_M$ values and quenching rates (f) of C2–C4. C1 could not be converged after R–W modeling, due perhaps to the weak or lack of quenching effect of this type of humic substances with SD. Therefore, we focused on changes in the $\log K_M$ and f values of C2–C4 before and after the soil infiltration treatment. While the $\log K_M$ of the protein component C3 was significantly increased in the influent and effluent water, its f value was significantly decreased. Therefore, the soil infiltration system improved the chemical stability of the complex between protein components and SD and increased the ability of these protein components to complex with SD (Yuan et al., 2017). Although the complex constants of the other components increased, their f values decreased to varying degrees. Therefore, protein-like components play a crucial role in the geochemical behavior of SD. This finding is consistent with 2D-COS results.

3. Conclusions

In the present study, soil infiltration was used to simulate the agricultural non-point source pollution runoff process, analyze the changes in DOM composition and complexation characteristics through spectral analyses (EEM-PARAFAC, SFS, and 2D-COS), and explore the mechanism and change process of SD–DOM complexation in non-point source pollution. We aimed to understand the migration of SD in the soil infiltration system and its impact on environmental risks. Four DOM components were identified using EEMs and PARAFAC. According to PCA, the pollution sources were livestock breeding wastewater and domestic sewage. Among the different components of DOM, SD produced a strong quenching effect on protein- and fulvic-like substances. Combined 2D-COS and SFS analyses showed that DOM was more sensitive to SD before than after the soil infiltration treatment, indicating that the improved soil system modified the order and ability of DOM and SD complexation. Furthermore, R–W modeling showed that hydrophobic protein substances play a pivotal role in complexation with SD. Simultaneously, the binding stability and sequence of fulvic-like substances were improved through soil infiltration. SD–DOM degrades as the DOM components are intercepted by the soil system, thereby reducing the concentration of SD entering the surface water environment and reducing the environmental risk of this antibiotic. Overall, spectroscopy is an ideal tool for evaluating the complexing ability of PPCPs with DOM and effectively predict their environmental risks.

Declaration of Competing Interest

The authors declare that they have no known competing financial interests or personal relationships that could have appeared to influence the work reported in this paper.

Acknowledgments

This work is supported by the National Water Pollution Control and Management Technology Major Project (No. 2018ZX07110005), the National Natural Science Foundation of China (No. 52170097), the Fundamental Research Funds for Beijing University of Civil Engineering and Architecture (No. X20137) and BUCEA Post Graduate Innovation Project (No. 2022).

Appendix A Supplementary data

Supplementary material associated with this article can be found, in the online version, at doi:10.1016/j.jes.2022.10.010.

REFERENCES

Awual, M.R., Yaita, T., Taguchi, T., Shiwaku, H., Suzuki, S., Okamoto, Y., 2014. Selective cesium removal from radioactive liquid waste by crown ether immobilized new class conjugate adsorbent. J. Hazard. Mater. 278, 227–235. doi:10.1016/j.jhazmat.2014.06.011.

Baghoth, S.A., Sharma, S.K., Amy, G.L., 2011. Tracking natural organic matter (NOM) in a drinking water treatment plant using fluorescence excitation-emission matrices and PARAFAC. Water Res 45, 797–809. doi:10.1016/j.watres.2010.09.005.

Bai, Y., Cui, Z.G., Su, R.G., Qu, K.M., 2018. Influence of DOM components, salinity, pH, nitrate, and bicarbonate on the indirect photodegradation of acetaminophen in simulated coastal waters. Chemosphere 205, 108–117. doi:10.1016/j.chemosphere.2018.04.087.

Bai, Y., Zhou, Y., Che, X., Li, C., Cui, Z., Su, R., et al., 2021. Indirect photodegradation of sulfadiazine in the presence of DOM: Effects of DOM components and main seawater constituents. Environ. Pollut. 268, 115689. doi:10.1016/j.envpol.2020.115689.

Bao, S., Wang, Z., Gong, X., Zeng, C., Wu, Q., Tian, B., et al., 2016. AgBr tetradecahedrons with co-exposed {100} and {111} facets: simple fabrication and enhancing spatial charge separation using facet heterojunctions. J. Mater. Chem. A 4, 18570–18577. doi:10.1039/C6TA06594E.

Chen, Z., Zhang, Y., Gao, Y., Boyd, S.A., Zhu, D., Li, H., 2015. Influence of dissolved organic matter on tetracycline bioavailability to an antibiotic-resistant bacterium. Environ. Sci. Technol. 49, 10903–10910. doi:10.1021/acs.est.5b02158.

Coble, P.G., 1996. Characterization of marine and terrestrial DOM in seawater using excitation-emission matrix spectroscopy. Mar. Chem. 51, 325–346. doi:10.1016/0304-4203(95)00062-3.

Focazio, M.J., Kolpin, D.W., Barnes, K.K., Furlong, E.T., Meyer, M.T., Zaugg, S.D., et al., 2008. A national reconnaissance for pharmaceuticals and other organic wastewater contaminants in the United States - II) Untreated drinking water sources. Sci. Total Environ. 402, 201–216. doi:10.1016/j.scitotenv.2008.02.021.

Göbel, A., McArdell, C.S., Joss, A., Siegrist, H., Giger, W., 2007. Fate of sulfonamides, macrolides, and trimethoprim in different wastewater treatment technologies. Sci. Total Environ. 372, 361–371. doi:10.1016/j.scitotenv.2006.07.039.

Guo, L., Lu, M., Li, Q., Zhang, J., Zong, Y., She, Z., 2014a. Three-dimensional fluorescence excitation-emission matrix (EEM) spectroscopy with regional integration analysis for assessing waste sludge hydrolysis treated with multi-enzyme and thermophilic bacteria. Bioresour. Technol. 171, 22–28. doi:10.1016/j.biortech.2014.08.025.

Guo, X.J., He, L.S., Li, Q., Yuan, D.H., Deng, Y., 2014b. Investigating the spatial variability of dissolved organic matter quantity and composition in Lake Wuliangsuhai. Ecol. Eng. 62, 93–101. doi:10.1016/j.ecoleng.2013.10.032.

Guo, X.J., Zhu, N.M., Chen, L., Yuan, D.H., He, L.S., 2015. Characterizing the fluorescent properties and copper complexation of dissolved organic matter in saline-alkali soils using fluorescence excitation-emission matrix and parallel factor analysis. J. Soils Sediments 15, 1473–1482. doi:10.1007/s11368-015-1113-7.

Guo, X., Li, C., Zhu, Q., Huang, T., Cai, Y., Li, N., et al., 2018. Characterization of dissolved organic matter from biogas residue composting using spectroscopic techniques. Waste Manag 78, 301–309. doi:10.1016/j.wasman.2018.06.001.

Hamscher, G., Pawelzick, H.T., Höper, H., Nau, H., 2005. Different behavior of tetracyclines and sulfonamides in sandy soils after repeated fertilization with liquid manure. Environ. Toxicol. Chem. 24, 861–868. doi:10.1897/04-182R.1.

Hernandez-Ruiz, S., Abrell, L., Wickramasekara, S., Chefetz, B., Chorover, J., 2012. Quantifying PPCP interaction with dissolved organic matter in aqueous solution: Combined use of fluorescence quenching and tandem mass spectrometry. Water Res. 46, 943–954. doi:10.1016/j.watres.2011.11.061.

Huang, Y., Tian, Y., Xie, L., Liu, Y., Dai, B., Guo, X., et al., 2020. The application of two-dimensional correlation spectroscopy for the binding properties of heavy metals onto digestate-derived DOM from anaerobic digestion of chicken manure. Ecotoxicol. Environ. Saf. 204, 111129. doi:10.1016/j.ecoenv.2020.111129.

Kokoszka, K., Wilk, J., Felis, E., Bajkacz, S., 2021. Application of UHPLC-MS/MS method to study occurrence and fate of sulfonamide antibiotics and their transformation products in surface water in highly urbanized areas. Chemosphere 283, 131189. doi:10.1016/j.chemosphere.2021.131189.

Lee, Y.K., Hong, S., Hur, J., 2021. Copper-binding properties of microplastic-derived dissolved organic matter revealed by fluorescence spectroscopy and two-dimensional correlation spectroscopy. Water Res 190. doi:10.1016/j.watres.2020.116775.

Li, Y., Pan, Y., Lian, L., Yan, S., Song, W., Yang, X., 2017. Photosensitized degradation of acetaminophen in natural organic matter solutions: the role of triplet states and oxygen. Water Res 109, 266–273. doi:10.1016/j.watres.2016.11.049.

Liang, Z., Yang, J., Zhou, C., Mo, Q., Zhang, Y., 2018. Carbon quantum dots modified BiOBr microspheres with enhanced visible light photocatalytic performance. Inorg. Chem. Commun. 90, 97–100. doi:10.1016/j.inoche.2018.02.013.

Liu, X., Liu, Y., Lu, S., Guo, W., Xi, B., 2018. Performance and mechanism into TiO 2 /Zeolite composites for sulfadiazine adsorption and photodegradation. Chem. Eng. J. 350, 131–147. doi:10.1016/j.cej.2018.05.141.

Luo, Y., Guo, W., Ngo, H.H., Nghiem, L.D., Hai, F.I., Zhang, J., et al., 2014. A review on the occurrence of micropollutants in the aquatic environment and their fate and removal during wastewater treatment. Sci. Total Environ. 473–474, 619–641. doi:10.1016/j.scitotenv.2013.12.065.

Navon, R., Hernandez-Ruiz, S., Chorover, J., Chefetz, B., 2011. Interactions of carbamazepine in soil: effects of dissolved organic matter. J. Environ. Qual. 40, 942–948. doi:10.2134/jeq2010.0446.

Noda, I., Ozaki, Y., 2005. Two-dimensional correlation spectroscopy - applications in vibrational and optical spectroscopy, two-dimensional correlation spectroscopy - applications in vibrational and optical spectroscopy. https://doi.org/10.1002/0470012404

Ohno, T., Bro, R., 2006. Dissolved organic matter characterization using multiway spectral decomposition of fluorescence landscapes. Soil Sci. Soc. Am. J. 70, 2028–2037. doi:10.2136/sssaj2006.0005.

Petrone, K.C., Fellman, J.B., Hood, E., Donn, M.J., Grierson, P.F., 2011. The origin and function of dissolved organic matter in agro-urban coastal streams. J. Geophys. Res. Biogeosciences 116. doi:10.1029/2010JG001537.

Ryan, D.K., Weber, J.H., 1982. Fluorescence quenching titration for determination of complexing capacities and stability constants of fulvic acid. Anal. Chem. 54, 986–990. doi:10.1021/ac00243a033.

Song, W.J., Fu, H.Y., Wang, G.Y., 2012. Study on a kind of Eco-concrete retaining wall's block with water purification function. Procedia Eng 28, 182–189. doi:10.1016/j.proeng.2012.01.703.

Sukul, P., Spiteller, M., 2006. Sulfonamides in the environment as veterinary drugs. Rev. Environ. Contam. Toxicol. 187, 67–101. doi:10.1007/0-387-32885-8_2.

Tedoldi, D., Chebbo, G., Pierlot, D., Kovacs, Y., Gromaire, M.C., 2016. Impact of runoff infiltration on contaminant accumulation and transport in the soil/filter media of Sustainable Urban Drainage Systems: A literature review. Sci. Total Environ. 569–570, 904–926. doi:10.1016/j.scitotenv.2016.04.215.

Wang, S., Yuan, R., Chen, H., Wang, F., Zhou, B., 2020. Effect of sulfonamides on the dissolved organic matter fluorescence in biogas slurry during anaerobic fermentation according to the PARAFAC analysis. Process Saf. Environ. Prot. 144, 253–262. doi:10.1016/j.psep.2020.07.033.

Wei, D., Li, M., Wang, X., Han, F., Li, L., Guo, J., et al., 2016. Extracellular polymeric substances for Zn (II) binding during its sorption process onto aerobic granular sludge. J. Hazard. Mater. 301, 407–415. doi:10.1016/j.jhazmat.2015.09.018.

Wu, M.H., Li, L., Liu, N., Wang, D.J., Xue, Y.C., Tang, L., 2018. Molybdenum disulfide (MoS2) as a co-catalyst for photocatalytic degradation of organic contaminants: a review. Process Saf. Environ. Prot. 118, 40–58. doi:10.1016/j.psep.2018.06.025.

Yang, L., Wang, T., Zhou, Y., Shi, B., Bi, R., Meng, J., 2021. Contamination, source and potential risks of pharmaceuticals and personal products (PPCPs) in Baiyangdian Basin, an intensive human intervention area. China. Sci. Total Environ. 760, 144080. doi:10.1016/j.scitotenv.2020.144080.

Yao, X., Zhang, Y., Zhu, G., Qin, B., Feng, L., Cai, L., et al., 2011. Resolving the variability of CDOM fluorescence to differentiate the sources and fate of DOM in Lake Taihu and its tributaries. Chemosphere 82, 145–155. doi:10.1016/j.chemosphere.2010.10.049.

Yao, Y., Li, Y.Z., Guo, X.J., Huang, T., Gao, P.P., Zhang, Y.P., et al., 2016. Changes and characteristics of dissolved organic matter in a constructed wetland system using fluorescence spectroscopy. Environ. Sci. Pollut. Res. 23, 12237–12245. doi:10.1007/s11356-016-6435-5 .

Yuan, D.H., Guo, X.J., Xiong, Y., Cui, J., Yin, X.A., Li, Y.Z., 2017. Pollutant-removal performance and variability of DOM quantity and composition with traditional ecological concrete (TEC) and improved multi-aggregate eco-concrete (IMAEC) revetment treatments. Ecol. Eng. 105, 141–149. doi:10.1016/j.ecoleng.2017.05.001.

Yuan, D.H., He, J.W., Li, C.W., Guo, X.J., Xiong, Y., Yan, C.L., 2019. Insights into the pollutant-removal performance and DOM characteristics of stormwater runoff during grassy-swales treatment. Environ. Technol. (United Kingdom) 40, 441–450. doi:10.1080/09593330.2017.1395481.

Yuan, D., Zhou, Q., An, Y., Guo, X., Chen, B., Wang, S.G., et al., 2019. Impacts of soil improvement on the pollutant-removal performance and DOM characteristics using a simulation experiment. Ecol. Indic. 105, 581–590. doi:10.1016/j.ecolind.2018.05.057.

Yuan, D.H., An, Y.C., He, X.S., Yan, C.L., Jia, Y.P., Wang, H.T., et al., 2018. Fluorescent characteristic and compositional change of dissolved organic matter and its effect on heavy metal distribution in composting leachates. Environ. Sci. Pollut. Res. 25, 18866–18878. doi:10.1007/s11356-018-2067-2.

Zhou, Y., Xiao, Q., Yao, X., Zhang, Y., Zhang, M., Shi, K., et al., 2018. Accumulation of terrestrial dissolved organic matter potentially enhances dissolved methane levels in Eutrophic Lake Taihu. China. Environ. Sci. Technol. 52, 10297–10306. doi:10.1021/acs.est.8b02163.